Chapter

Structural Characteristics and Magnetic Properties of Al_2O_3 Matrix-based Co-cermet Nanogranular Films

Nguyen Anh Tuan* and Giap Van Cuong

International Training Institute for Material Science (ITIMS), Hanoi University of Science and Technology (HUST), Vietnam

***Corresponding Author:** Nguyen Anh Tuan, International Training Institute for Material Science, Hanoi University of Science and Technology, Hanoi 10000, Vietnam.

First Published **January 21, 2019**

This Book Chapter is an excerpt from an article published by Nguyen Anh Tuan, et al. at Journal of Materials in October 2015. (Giap Van Cuong, Nguyen Anh Tuan, Nguyen Tuan Anh, et al., "Structural Characteristics and Magnetic Properties of Al2O3 Matrix-Based Co-Cermet Nanogranular Films," Journal of Materials, vol. 2015, Article ID 834267, 8 pages, 2015. https://doi.org/10.1155/2015/834267.)

Conflict of Interests: The authors declare that there is no conflict of interests regarding the publication of this paper.

Abstract

Magnetic micro- and nanogranular materials prepared by different methods have been used widely in studies of magneto-optical response. However, among them there seems to be nothing about magnetic nanogranular thin films prepared by a *rf* co-sputtering technique for both metals and insulators till now. This paper presented and discussed on preparation, structural characteristics, and magnetic properties of alumina (Al_2O_3) matrix-based granular Co-cermet thin films deposited by means of the cosputtering technique for both Co and Al_2O_3. By varying the ferromagnetic (Co) atomic fraction, x, from 0.04 to 0.63, several dominant features of deposition for these thin films were shown. Structural characteristics by X-ray diffraction confirmed a cermet-type structure for these films. Furthermore, magnetic behaviours presented a transition from paramagnetic- to superparamagnetic- and then to ferromagnetic-like properties indicated an agglomeration and growth following Co components of Co clusters or nanoparticles. These results shown a typical granular Co-cermet feature for the Co-Al_2O_3 thin films prepared, in which Co magnetic nanogranules are dispersed in a ceramic matrix. Such nanomaterials can be applied suitably for our investigations in future on the magneto-optical responses of spinplasmonics.

Introduction

Cermet, or ceramic metal, is a kind of composite material in which many component phases co-exist. Normally, it includes metal-

lic and ceramic phases that are separated and mixed. Al_2O_3 matrix-based granular Co-cermet can form by means of immersing segregated Co nanoparticles into an alumina matrix, Al_2O_3. In other words, this is a kind of nanocomposite consisting of metallic nanoparticles embedded in an insulating (or even metallic) matrix. Alumina-based ceramics (Al_2O_3) possess excellent physical and chemical properties, as well as good mechanical resistance and thermal stability. Nanogranular composite materials display a particularly rich variety of interesting physical properties, including conducting, optical, magnetic, and so on. [1].

The materials of this type are quite suitable for different aims of research. For example, formerly, Au tiny particles dispersed into a dielectric medium have been considered as optical media to study on plasmonics [2]. In the field of magnetic materials, the Co-cermet thin film is also called magnetic granular film (MGF) because of the ferromagnetic and nanogranular structural characteristics of Co. Such materials are estimated to open a new opportunity for developing novel soft magnetic materials [3]. In electronics and spintronics, Al_2O_3 matrix-based Co-cermet MGFs, such as Co-Al_2O_3 films, have been also known to have the spin-dependent magnetic tunneling effect [4,5] and a very typical feature by the Coulomb blockade phenomenon for the inter-granules magnetic tunnel [6]. Furthermore, the MGF material has been recently reported to still exhibit rectification [7]. In addition, MGFs are predicted they can also be appropriate for studying magnetic field-dependent super-*k* dielectric granular and spin-caloritronic materials.

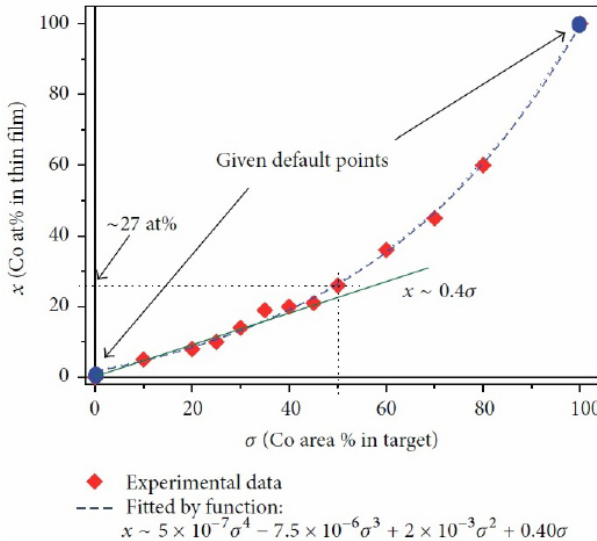

Figure 1: Co content of Co-Al_2O_3 thin films, x, as a function of Co:Al_2O_3 area ratio in the target, σ. Points in zero (origin) and 100% coordinates are as given default data.

Recently, it has been observed interesting phenomena in nano-magnetic materials, such as spin-plasmonic propagation in a system including gold-plated ferro-magnetic micro-particles [8], excitation of surface plasmons on magnetoactive materials [9], or enhancement of surface plasmon of metal nanocomposite films [10]. However, among the materials structured from metallic nano-particles dispersing in a dielectric matrix for studying on spin-plasmonics or other nanomagneto-optical responses, those prepared using radio-frequency (*rf*, 13.56 MHz) cosputtering techniques for both ferromagnetic metals and dielectric isolators seem to be unreported as yet. For example, CoFe-Al_2O_3 granular films, which are similar to our Co-Al_2O_3 granular films, were coevaporated using *e*-beam evaporation for studies of IR reflectance and magnetorefractive effects [11]. Recently, some kind of nanomaterials for the magnetic photonics or plasmonic

resonance studies were fabricated using different techniques, such as sol-gel method for magnetic photonic crystals based on Fe_3O_4 nanoparticles [12], spray pyrolysis technique for Au nanoclusters embedded in titania (TiO2) matrix [13], thermal evaporation method then annealed at high temperature for Au nanoparticles [14], ect. Based on those studies, we were motivated to preparate Al_2O_3 matrix-based Co-cermet MGF materials using *rf* cosputtering technique. These cermet films are believed to be able to excellently satisfy to study plasmonic resonance phenomena, and especially the spin-dependent optical response as an approach to the field of spinplasmonics.

In this paper, we report on the preparation and analysis of several typical characteristics of deposition and the structural and magnetic properties of Co-Al_2O_3 cermet films as a function of Co content.

Experimental Details

The samples of Co_x-$(Al_2O_3)1-_x$ cermet films were deposited onto 200-μm thick lamellar glass substrates via *rf* cosputtering technique (Alcatel SCM 400) at ambient temperature. The background vacuum was about 10^{-9} bar and argon gas of 5N purity was used as the sputter gas kept constant at a pressure of ~ 5×10^{-6} bar during the sputtering time. A 4N-alumina disk of 7.5 cm diameter with 4N-Co pieces pasted on its surface was used as a target, and a sputtering power of 300 W was applied. The target-to-substrate distance is 7.5 cm, and the rf power density was evaluated of about 7 W/cm^2. The Co and Al_2O_3 depositing rates were 0.5 and 0.2 Å/s, respectively, and an average depositing rate for Co-Al_2O_3 was determined to be about 0.3 Å/s. The film thickness was varied from ~90 to 100 nm and was measured using an Alpha-Step IQ by KLA Tencor. Co contents with x = 0.04–0.63, which correspond with 4–63 Co at.%, were determined *via* energy dispersive X-ray spectroscopy (EDS), and the morphology of the film surfaces was observed via scanning electron microscopy (SEM) by using JEOL JSM-541. In particular cases, the surface morphology of several selected samples was also observed using an atomic force microscopy (AFM) model FlexAFM by Nanosurf. The crystalline structural characteristics of the Co-Al_2O_3 cermet films were investi-

gated via X-ray diffraction (XRD) by using a Philips X'Pert PRO with Cu-Kα radiation (λ = 1.5406 Å) for two theta values from 10° to 80°. Measurements of the magnetic properties were carried out at room temperature by using a magnetometer MicroMag 2900/3900, essentially at magnetic fields parallel to the film plane and up to 14 kOe.

Results and Discussion

The Co-Al_2O_3 thin films were deposited via co-sputtering from a-combined target including different Co (A_{Co}) and Al_2O_3 (A Al_20_3) areas that have different sputtering rates, such as 190 and 40 Å/s, respectively [15]. Other factors still affect the deposition processes of the thin films, such as reflection, re-sputtering, and desorption, and the sputte-ring yield of Co is higher than that of Al_2O_3, which corresponds to 1.4 versus 0.4 atoms/ion, respectively [15]. Therefore, the Co content in the thin films is not identical to that in the target. Figure 1 shows a relationship between the Co content x determined via EDS in the thin films (in at.%) and Co:Al_2O_3 area ratio in target, σ = ACo/A Al_20_3 (in area percent). The experimental data fitted very well to a fourth-order law, which is defined approximately by the equation $x \approx 5\times10^{-7}\sigma^4 - 7.5\times10^{-6}\sigma^3 + 2\times10^{-3}\sigma^2 + 0.40\sigma$. The result shows also that for $x \leq 0.4$, the Co atom amount in the films versus Co area in the target can obey very well a first-order relation, i.e., $x \approx 0.40\sigma$. This means the Co amount increased more proportionally with a trend of an uncompleted fourth-order polynomial function, or almost exponentially with a law of $x \sim \{\exp[(0.02\sigma + 0.5)] - 1\}$. The fourth-order relation between A_S/A_T areal ratio of substrate electrode (A_S) and target electrode (A_T) and the V_T/V_S potential ratio of the potential on the target (cathode) sheath (V_T) and substrate sheath (V_S), i.e. $V_T/V_S = (A_S/A_T)^4$ [16] mainly governs this behavior of growth rate of Co atom amount in the film. The increase in Co-chip area stuck on the Al_2O_3 target, or the increase of the σ ratio, is also synonym with the strong enhancement of an effective potential fallen on cathode, i.e., V_T sheath potential, in the sputtering process for Co because the sputtering yield of Co is very high compared to that of Al_2O_3. Thus, the ion bombardment of the substrate for re-sputtering and desorption of Co atoms, which had been absorbed on substrate, was minimized.

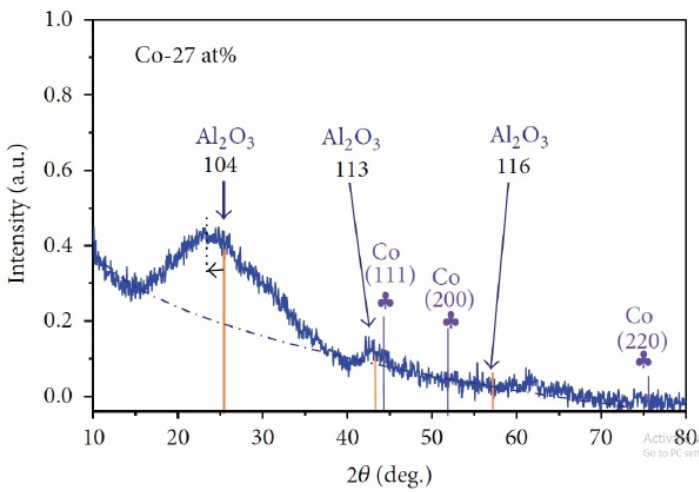

Figure 2: XRD pattern of $Co_x(Al_2O_3)_{1-x}$ thin film typically selected with $x = 0.27$. Dotted line presents background signal from the glass substrate. Violet and orange lines show standard XRD lines for Co and Al_2O_3, respectively. The shift from the Al_2O_3 (104) line of the biggest hump is pointed out.

Figure 2 shows a typical XRD pattern selected for the sample with x = 0.27. The XRD pattern presents a superposition of the signal caused by the Co-Al_2O_3 thin film (blue full line), called diffractogram, and the contribution of the glass substrate (illustrated by the dotted line), or from other background spectra/signals. The figure shows that the Al_2O_3 matrix dominantly had a typical amorphous-like phase or a low crystalline structure with a large hump at around 2θ ~25° and a small one at ~43°. Three strongest standard peaks for bulk α-Al_2O_3 crystal corresponding to (104), (113), and (116) Miller indexes are indicated by orange lines in Figure 2. These standard peaks pertain to

the rhombohedral system of the α-Al_2O_3 for structure as indicated in the JCPDS-International Centre Diffraction Data Card number 46-1212. However, the coinci-dence of these peaks with the amorphous-like humps of Al_2O_3 shows that the Al_2O_3 matrix of the samples varied from a rhombohedral crystal structure into a disordered variant. Alternatively, the large hump also presents a type of the so-called fine crystalline structure. When Scherrer's formula is used

$$D = \frac{0.94\lambda}{\beta \cos\theta} \quad , \quad (1)$$

where D is the average crystallite size, λ is the X-ray wavelength of CuK_α radiation, β is the full width of half maximum (FWHM) of the diffraction peaks, and θ is the diffraction angle, the mean size of the Al_2O_3 fine crystallites was found to be about 1 nm or ~ 10 Å. Given below the ion radii of Al^{3+} and O^{2-} in an Al_2O_3 molecular, each fine crystallite includes only about 10 molecules. Hence, the Al_2O_3 matrix can be considered as a mixture of fine crystallite and amorphous phases.

On the other hand, a rather clear shift was observed for the Al_2O_3 humps from standard peak positions towards the left side, which corresponds to a lower-2θ angle. The results seem to indicate a tensile stress in the Al_2O_3 matrix. This lattice deformation or disorder in the rhombohedral structure may be due to Co atoms or clusters dispersing into the matrix because the ion radius of Co^{2+}, ~ 0.075 Å, is larger than that of Al^{3+}, ~ 0.054 Å, but smaller than that of O^{2-}, ~ 0.140 Å (in terms of atomic radius, Co ~ 0.152 Å, and Al ~ 0.118 Å, O ~ 0.048 Å) [17]. In other words, the shift of the Al_2O_3 humps is indicative of the existence of Co atoms in the rhombohedral lattice of Al2O3 or Co clusters in the Al2O3 matrix. The indication of the shift for matrix diffraction peaks has been used as an experimental evidence supporting, for example, a continuos solid solution of interstitial intermetallics [18], or an insertion of atoms of a certain metal (e.g Co) into a matrix

metal (e.g Cu) by means of a ion implantation [19]. A similar trend of the shift of the MgO Bragg diffraction peaks (i.e. matrix phase) compared to the peak positions in the pure MgO XRD patterns when adding another metals (e.g Al, Cr, Ti, Zr) to the MgO matrix phase has been also observed [20].

As seen in Figure 2, almost no clear signature of the Co peaks was observed, except for a very small hump at around $2\theta \sim 44°$. The three strongest standard peaks of Co-fcc crystal corresponded to the (111), (200), and (220) Miller indexes, as indicated by violet lines with rosette figures in Figure 2 (after JCPDS-ICDD card No. 01-089-7093), where the Co-fcc (111) line coincides with the small hump right beside the Al_2O_3 (113) hump. There are two main arguments for this absence of Co peaks. First, X-ray fluorescent radiation from Co was the one used to be excited in the sample by the Cu-Kα radiation of the used X-ray source. The background of an XRD pattern is composed of many variant factors, in which there are fluorescent radiation and small particles [21]. Co is a ferromagnetic element that is known to cause the strongest X-ray fluorescent for Cu-Kα radiations. Thus, the fluores-cent effect may cause the weakest Co diffraction peaks so that the peaks become almost invisible in relation to the background in the XRD spectra [22]. Second, this reason can occur simultaneously with the first reason but can also be more dominant: the shift of the Al_2O_3 humps as mentioned above, the size of Co clusters is very small, and/or the Co atoms are broadly dispersed into the Al_2O_3 matrix. Such similar feature of no diffraction peaks in the XRD has been also observed for amorphous or nano-crystalline CoFe clusters in a SiO_2 silica matrix, with cluster sizes of about 1 nm – 4 nm observed and estimated based on their TEM images [23]. The Co particle sizes of the Co-cermet films are hard to evaluate from the XRD data by using Scherrer's formula because of the very weak X-ray reflection of Co. However, a raw estimation can be carried out from the superparamagnetic (SPM) behavior of the Co-Al_2O_3 thin films, which we will

discuss below. The result shows the same sizes. A redundant amount of about 5% volume of Co atoms that will not participate in the formation of Co particles/clusters is mentioned. These redundant Co atoms in the amorphous state created the shift in the XRD peaks. A similar shift behavior of the diffraction peaks caused by the doping of Co atoms into TiO_2 nanoparticles has been pointed out [24]. For metal–insulator systems, such as Co-Al_2O_3, separation and isolation of metallic clusters or particles in the oxide matrix can occur easily, because the large difference between the surface energies of Co and Al_2O_3 leads to an isotropic three-dimensional growth of Co [25,26]. However, it is difficult to determine the size of Co particles by using Scherrer's formula (1) in this situation due to no clear Co XRD peaks, as seen. But it can be estimated by means of magnetization behaviors in case of superparamagnetism, as seen hereinafter.

Figure 3(a) shows a rather rough surface topographic morphology of the as-deposited Co-Al_2O_3 thin film selected at $x = 0.27$ as an example. Figs. 3(b) and (c) present the surface AFM images (size: 20 μm × 20 μm) captured in the amplitude type for the same sample, which correspond to the as-deposited and after annealing at 250 °C for 1 h, respectively. The rough surface is caused by the low atomic mobility due to deposition at room temperature. The as-deposited thin films seem to be improved after annealing. As seen from the line fit indicated in Figs. 3(b) and (c), the height amplitude range was reduced from 33 nm to 14 nm.

Dominant features in the change in the magnetic phases from paramagnetic- to superparamagnetic- and ferromagnetic-like behaviors with increasing Co content, which correspond to $x < 0.12$, $0.12 \leq x < 0.37$, and $x \geq 0.37$, respectively, were observed for all Cox-(Al_2O_3)1-x granular thin films prepared. For systems with Co granules immersed in non-magnetic matrixes, the ferromagnetic behavior begins to appear at room temperature with a concentration at ~ 35 Co at.% [27]. Figure 4(a) presents only several typical normalized *M(H)* magnetization curves selected for the $Co_xAl_2O_3$ thin films with

x = 0.06, 0.16, 0.27, and 0.49, which are representative of the three regions of magnetic phases. A paramagnetic-like behavior at room temperature with an unsaturated sign of up to about 1.4 T (Tesla) was observed, and no hysteresis was observed in the case of x = 0.06. This result can imply that the matrix of the film was sprinkled with Co atoms or with very small atomic agglomerates. In fact, because Co clusters are formed only part from the Co material and the remainder is dispersed in non- or weak-magnetic states buried within the Al_2O_3 matrix, the true concentration of the magnetic clusters is somewhat lower than the one determined from EDS [28]. For Co-Al_2O_3 films, Co atoms are atomically dispersed in the Al_2O_3 matrix and, as mentioned above, can hold an amount up to 5 vol.% [29]. The *M(H)* curve in this case can reflect a dominant feature of the spin glass state because Co atoms seam to behave individually. Moreover, a drastic competition between magnetostatic energy, thermal fluctuation, and RKKY-type interaction is reality. For x = 0.16 and 0.27, the *M(H)* curves expressed in Figure 4(a) show typical room temperature SPM behaviors. This type expresses a granular system of almost non-interactive single domain spherical ferromagnetic particles. For uniform particle size d, the magnetization curve *M(H)* is described by the Langevin function:

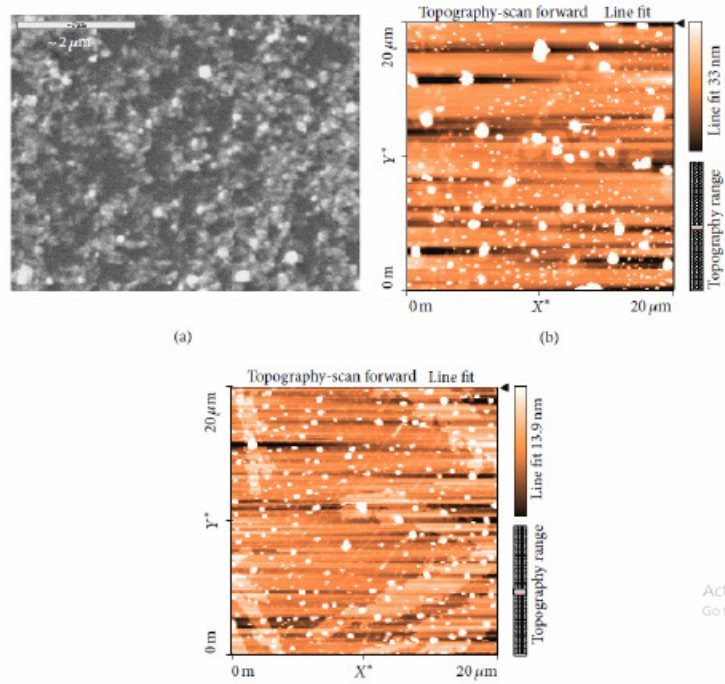

Figure 3: (a) Surface SEM image of as-deposited Co-Al_2O_3 thin film with x = 0.27. (b) AFM image 20 μm × 20 μm for the surface of the as-deposited $Co_{0.27}$-Al_2O_3 film, and (c) of the film after annealing at 250 °C for 1 hour.

$$M(H) = M_S L(\alpha) = M_S\left(\coth\alpha - \frac{1}{\alpha}\right), \text{ with } \alpha = \frac{M_S VH}{k_B T} \quad , \quad (2)$$

where MS is the saturation magnetization of ferromagnetic particles with volume $V = (4\pi/3)(d/2)^3$, k_B is Boltzmann constant, and T is temperature. In fact, there are size distributions in SPM particles. Thus, the total magnetiza-tion is better described as a weighted sum of Langevin functions under the form of Eq.(2) [30]. However, a small hysteresis behavior of SPM status, with coercivity up to HC ~ 8.6 mT but with a very low remanence, Mr < 5 % was observed for the case of

x = 0.27, as seen in Figure 4(b). This result proves that there can be a weak interaction between Co particles, such as a dipolar intergranular interaction that resulted in anisotropy in the system [31]. It can be also due to a slight shape and/or crystal anisotropy in these particles [32]. Figure 5 presents a typical investigation of hysteresis loops for the case of x = 0.27 with both configurations of H paralell and perpendicular to the plane of this sample. As seen, two magnetiztion curves are almost identical. This shows a rather isotropic behaviour for the Co particles. However, a linearity at low-H region (< 0.25 T) of the magnetiztion curve measured in the perpendicular configuration presents a little in-plane anisotropy with the anisotropic field H_A of about 0.25 T (~ 2.5 kOe). In other words, the Co particles have an somewhat oblate spherical form.

With above features, Co particle sizes can be assigned to the range of about 1 nm – 5 nm in diameter [32]. Given formula $T_B = VK_{Co}/25k_B$, below which the magnetization will be stable, for constant size spherical particles, the blocking temperatures T_B of the SPM Co-cermet systems can be roughly established. For $k_B = 1.381\times10^{-16}$ erg.K^{-1} and $K_{Co} = 4.1\times10^6$ erg/cm3 at room temperature for Co [33] for particles that are distributed from 1 nm – 5 nm in particle size, T_B will be in a broad range from 0.6 K to 80 K. For instance, for d = 3 nm, T_B ~ 17 K. Such systems will correspond to the SPM relaxation time $\tau < 10^5$ s [32]. If using the ion radius as has given for Co^{2+}, the number of Co atoms in each particle in this range of size can be estimated about 250×10^3 to 35×10^6. Several studies on systems of Co-based granular thin films have also confirmed these sizes via transmission electron micrograph (TEM) [29,34] or scanning tunneling micro-scopy (STM) [35,36], and via calculations from the Langevin fitting of SPM *M-H* data [29,37]. Therefore, in this case, a state called the spin cluster state and/or a Co-rich particle state of Co atoms in the Al_2O_3 matrix can also show up. The oscillation-type RKKY interaction between Co clusters can be brought into play, similar to type of granular metallic alloys, such as Fe-Cr alloys [38].

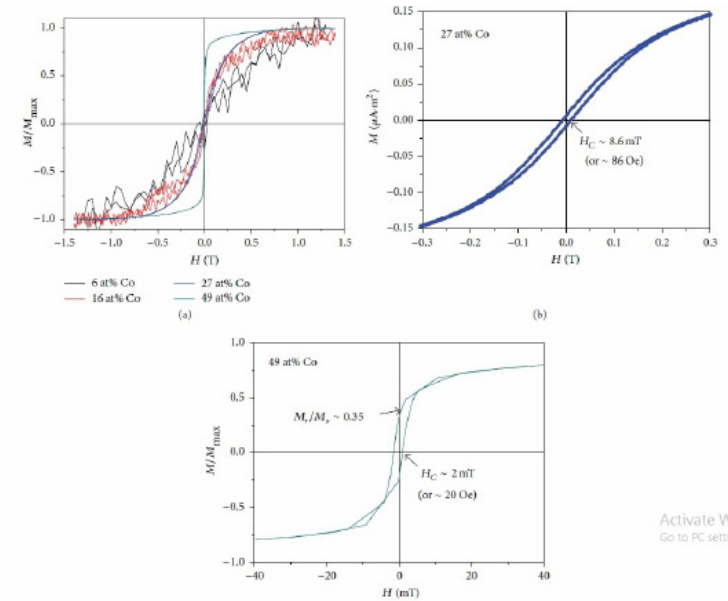

Figure 4: Room temperature magnetization curves *M(H)* of $Cox(Al_2O_3)_{1-x}$ thin films with: (a) x = 0.06, 0.16, 0.27, and 0.49. (b) *M(H)* curve extracted partly in a range ±0.3 T for the case of Co-27 at% thin film presents a narrow hysteresis loop with H_C ~ 8.6 mT and very small remanence. (c) A small hysteresis loop with H_C ~ 2 mT and ratio (M_r/M_s) ~ 0.35 for the case of Co-49 at.% thin film.

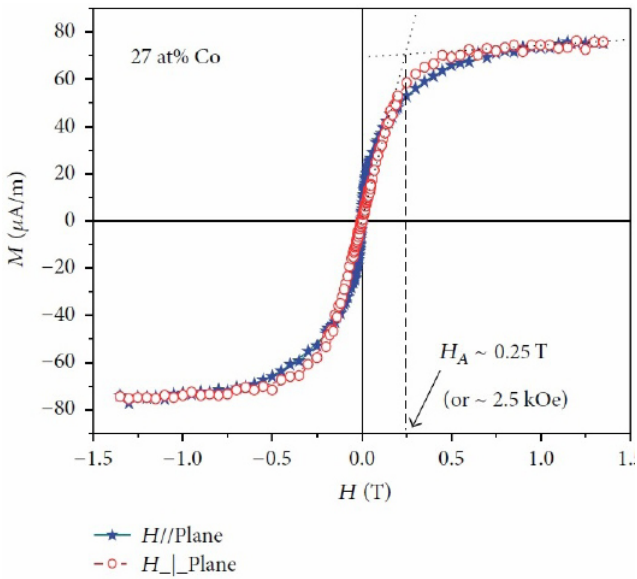

Figure 5: Magnetization curves *M(H)* measured in both configurations with H paralell and perpendicular to the plane of $Co_{0.27}(Al_2O_3)_{0.73}$ thin film. An anisotropic field H_A of about 0.25 T (~ 2.5 kOe) for the perpendicular configuration can be determined.

When the Co content is high as 49 at.%, a ferromagnetic type in the *M(H)* curve showed a narrow hysteresis loop with H_C ~ 2 mT, and the ratio of remanent and saturation magnetization (M_r/M_S) was estimated to be almost ~ 0.35, as inserted in Figure 4(c). These behaviors of the weak coercivity and the remanence near 0.5 M_S prove that the Co particles can be still in ferromagnetic nature at room temperature with an essential single domain form and are randomly dispersed. Both coercivity and ratio (M_r/M_s) = 0.5 (theoretically) are signature/ evidence for a random dispersion of non-interacting single domain particles but in weakly blocked state of particle magnetization [1,39]. For granular metal systems, there exists a so-called percolation

threshold (x_p) of the volume fraction at which the first continuous metal particle is formed [1,40]. This threshold is around 50%–60% for the Co particles in an amorphous Al-O matrix [1,34]. For higher Co contents with x = 0.49 and below the percolation threshold, the Co particles are inclined to agglomerate into larger Co-rich regions or masses, in which each composed particle is still almost separated from the others but is coupled (or blocked) magneto-statically together in a ferromagnetic- type state, which is that similar to real ferromagnetic entities. To some extent, the ferromagnetic-type property with a weak coercivity of such assemblies of nanoparticles can therefore be considered as a so-called super-ferromagnetic (SFM) state, as called at first by Bostanjoglo and Roehkel [41]. This way of looking at the SFM state is similar to the case of calling of the SPM-type state. Thus, the magnetization process for such systems should occur in two steps: (i) in low-field region, about several tens of oersted, orientation of magnetization of the large ferromagnetic masses; (ii) in higher-field region, orienta-tion along the applied field of the disorder magnetization of the clusters/particles that are dispersed in the matrix and/or in the ferromagnetic masses. These two steps will correspond with two magnetization components that can be separated for each ferromagnetic and paramagnetic contribution [27].

When the particle concentration is further increased, the magnetic interparticle interactions become non- negligible and one may find a crossover from single-particle blocking to collective freezing. When the Co content is high enough over the percolation threshold, such as for x = 0.63, the Co clusters/particles are impinged on each other or the infinite cluster/particle occupies almost the whole volume of the sample [31,33], where the magnetic properties are close to the ones of bulk ferromagnetic Co films.

Conclusion

We have fabricated the Co-Al_2O_3 films by rf cosputtering onto glass substrates with a rather high rf power density. We found that at such the sputtering condition the relationship between the Co con-

tents in the Co-Al_2O_3 films and the Co area ratio in the target obeyed a quaternary polynomial function, and these films hold dominant features of a typical nanocomposite cermet. The Co-Al_2O_3 films, which can be called as Al_2O_3 matrix-based Co-cermet nanogranular films, have shown that the amorphous Al_2O_3 ceramic matrixes were sprinkled with Co magnetic atoms, clusters or nanoparticles, depending on Co contents. The important manifestations of a cermet-type nanogranular structure are the shift of XRD peaks from standard peaks for pure matrix phase, e.g. Al_2O_3, due to internal microstress caused by Co atoms and/or clusters or particles, and magnetic behaviours among the paramagnetism pass superparamagnetism to weak ferromagnetism for magnetic phase, e.g. Co, due to spin glass or cluster glass states caused by ferromagnetic superfine particles. Such the cermet-type nanogranular films are suitable to study on spin-plasmonics.

Acknowledgements

This research is funded by Vietnam National Foundation for Science and Technology Development (NAFOSTED) under grant number 103.02.2012.65.

References

1. CL Chien. Granular magnetic solids. Journal of Applied Physics. 1991; 69: 5267–5272.
2. SA Maier, HA Atwater. Plasmonics: Localization and guiding of electromagnetic energy in metal/dielectric structures. Journal of Applied Physics. 2005; 98: 011101.
3. DP Yang, YD Zhang, S Hui. Mössbauer spectroscopic and x-ray diffraction studies of Fe/SiO2 nanocomposite soft magnetic materials. Journal of Applied Physics. 2002; 91: 8198–8200.

4. H Fujimori, S Mitani, S Ohnuma. Tunnel-type GMR in Co-Al-O insulated granular system – Its oxygen-concen-tration dependence. Journal of Magnetism and Magnetic Materials. 1996; 156: 311–314.

5. S Mitani, H Fujimori, K Takanashi, K Yakushiji, JG Ha, et al. Tunnel-MR and spin electronics in metal–nonmetal granular systems. Journal of Magnetism and Magnetic Materials. 1999; 198–199: 179–184.

6. Jun-ichiro Inoue. In: Teruya Shinjo, editor. GMR, TMR and BMR. Nanomagnetism and Spintronics. Amsterdam: Elsevier. 2009; 69.

7. Nguyen Tuan Anh, Giap Van Cuong, Nguyen Anh Tuan. Diode-like behaviorof I–V curves of CoFe–(Al–O)/Si(100) granularthin films. Journal of Magnetism and Magnetic Materials. 2015; 374: 463–468.

8. KJ Chau, M Johnson, AY Elezzabi. Electron-Spin-Dependent Terahertz Light Transport in Spintronic-Plasmonic Media. Physical Review Letters. 2007; 98: 133901.

9. L Sapienza, D Zerulla. Surface plasmon excitation on magnetoactive materials. Physical Review B. 2009; 79: 033407.

10. V Singh, P Aghamkar. Surface plasmon enhanced third-order optical nonlinearity of Ag nanocomposite film. Applied Physics Letters. 2014; 104: 111112.

11. D Bozec, VG Kravets, JAD Matthew, SM Thompson, AF Kravets. Infrared reflectance and magnetorefractive effects in metal–insulator CoFe–Al_2O_3 granular films. Journal of Applied Physics. 2002; 91: 8795-8797.

12. Mei Fang. Licentiate Thesis: 3D magnetic photonic crystals: Synthesis and Characteriszation, Royal Institute of Technology, School of Industrial Engineering and Management, De-

partment of Materials Science and Engineering, Division of Engineering Materials Physics SE-100 44 Stockholm. Sweden: Stockholm. 2010.

13. P Kumar, MM Ahmad. Plasmonic resonance in spray deposited Au nanoparticles grown on TiO2 thin film. Advced Materials Letters. 2015; 6: 628-632.
14. M Brodyn, V Volkov, V Lyakhovetsky, V Rudenko, V Styopkin. Femtosecond optical nonlinearity of Au nanoparticles under their excitation in nonresonant relative to surface plasmon conditions. Appl. Phys. B. 2013; 111: 567–572.
15. http://www.semicore.com/reference/sputtering-yields-reference.
16. M Ohring. The Materials Science of Thin Films. Cambridge: Academic Press, Inc. San Diego: Harcourt Brace Jovanovich, Publishers. 1992; 123.
17. http://www.webelements.com.
18. JMD Coey. Interstitial intermetallics. Journal of Magnetism and Magnetic Materials. 1996; 159: 80–89.
19. H Errahmani, A Berrada, S Colis, G Schmerber, A Dinia, et al. Structural and magnetic studies of CoCu granular alloy obtained by ion implantation of Co into a Cu matrix, Nuclear Instruments and Methods in Physics Research Section B: Beam Interactions with Materials and Atoms. 2001; 178: 69–73.
20. M Saraiva. Sputter Deposition of MgO Thin Films: The Effect of Cation Substitution, PhD. Thesis, ISBN 978-94-6197-038-1, Universiteit Gent, Belgium. 2012; 65–70.
21. SJ van der Gaast, AJ Vaars. A method to eliminate the background in X-ray diffracion patterns of oriented clay mineral samples, Clay Minerals. 1981; 16: 383–393.

22. BD Cullity, SR Stock. Elements of X-ray diffraction, Third Edition. New Jersey: Prentice Hall, Inc. 2001; 255-257.

23. H Kumar, S Ghosh, D Bürger, Lin Li, SQ Zhou, et al. Role of Coulomb blockade and spin-flip scattering in tunneling magnetoresistance of FeCo-Si-O nanogranular films. Journal of Applied Physics. 2011; 109: 073914.

24. B Choudhury, A Choudhury, AKM Maidul Islam, P Alagarsamy, M Mukherjee. Effect of oxygen vacancy and dopant concentration on the magnetic properties of high spin Co^{2+} doped TiO_2 nanoparticles. Journal of Magnetism and Magnetic Materials. 2011; 323: 440–446.

25. LF Schelp, A Fert, F Fettar, P Holody, SF Lee, et al. Vaurès, Spin-dependent tunneling with Coulomb blockade. Physical Review B. 1997; 56: R5747.

26. F Fettar, SF Lee, F Petroff, A Vaures, P Holody, et al. Temperature and voltage dependence of the resistance and magnetoresistance in discontinuous double tunnel junctions. Physical Review B. 2002; 65: 174415.

27. MB Stearns, Y Cheng. Determination of para and ferromagnetic components of magnetization and magnetoresistance of granular Co/Ag films. Journal of Applied Physics. 1994; 75: 6894–6899.

28. CJ O'Connor, VO Golub, A Ya. Vovk, AF Kravets, AM Pogoriliy. Influence of Particle Size Distribution in Cermet Nanocomposites on Magnetoresistance Sensi-tivity. IEEE Transactions on Magnetics. 2002; 38: 2631–2633.

29. GA Niklasson, CG Granqvist. Optical properties and solar selectivity of coevaporated Co-Al_2O_3 composite films. Journal of Applied Physics. 1984; 55: 3382–3410.

30. FC Fonseca, GF Goya, RF Jardim, R Muccillo, NLV Carrenõ, et al. Superparamagnetism and magnetic properties of Ni nanoparticles embedded in SiO_2. Physical Review B. 2002; 66: 104406.

31. D Kechrakos, KN Trohidou. Interplay of dipolar interactions and grain-size distribution in the giant magnetoresistance of granular metals. Physical Review B. 2000; 62: 3941–3951.

32. BD Cullity. Introduction to magnetic materials. Menlo Park: Addison-Wesley Pub. Co., Inc. 1972; 383–389.

33. RC O'Handley. Modern magnetic materials - Principles and Applications. New Jersey: John Wiley & Sons, Inc. 2000; 192.

34. M Ohnuma, K Hono, H Onodera, S Ohnuma, H Fujimori, et al. Microstructures and magnetic properties of Co–Al–O granular thin films. Journal of Applied Physics. 2000; 87: 817–823.

35. K Takanashi, S Mitani, J Chiba, H Fujimori. Scanning tunneling microscopy investigation of single electron tunneling in Co–Al–O and Cu–Al–O granular films. J. Appl. Phys. 2000; 87: 6331.

36. S Mitani, K Takanashi, K Yakushiji, J Chiba, H Fujimori. Study on spin dependent tunneling and Coulomb blockade in granular systems with restricted tunneling paths. Mate. Sci. Eng. 2001; B24: 120.

37. RW Chantrell, J Popplewell, SW Charles. Measure-ments of particle size distribution parameters in ferrofluids. IEEE Transactions on Magnetics. 1978; 14: 975–977.

38. T Sugawara, K Takanashi, K Hono, H Fujimori. Study of giant magnetoresistance behavior in sputter-deposited Cr-Fe alloy films. Journal of Magnetism and Magnetic Materials. 1996; 159: 95–102.

39. A Dzarova, F Royer, M Timko, D Jamon, P Kopcansky, et al. Magneto-optical study of magnetite nanoparticles prepared by chemical and biomineralization process. Journal of Magnetism and Magnetic Materials. 2011; 323: 1453–1459.

40. Aya, Vovk JQ Wang, AM Pogoriliy, OV Shypil, AF Kravets. Magneto-transport properties of CoFe-Al_2O_3 granular films in the vicinity of the percolation threshold. Journal of Magnetism and Magnetic Materials. 2002; 242-245: 476–478.

41. O Bostanjoglo, K Roehkel. Superferromagnetism in gadolinium films. Physica status solidi (a). 1972; 11: 161-166.